PREPRINT UCRL- 77045

Conf-751130--12

Lawrence Livermore Laboratory

FUSION TARGETS DESIGNED TO MATCH PRESENT RELATIVISTIC ELECTRON BEAM MACHINE PARAMETERS

D. J. Meeker, J. H. Nuckolls, R. O. Bangerter

This paper was prepared for presentation at
The American Physical Society Meeting, Plasma Physics Division
St. Petersburg, Florida, Nov. 10-14, 1975

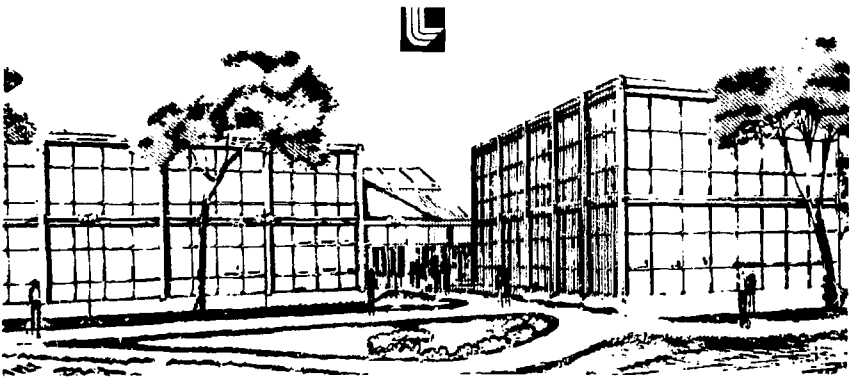

FUSION TARGETS DESIGNED TO MATCH PRESENT RELATIVISTIC ELECTRON BEAM MACHINE PARAMETERS*

D. J. Meeker, J. H. Nuckolls, R. O. Bangerter
University of California, Lawrence Livermore Laboratory, Livermore, California 94550

I. Introduction

Recent advances in electron beam accelerator technology have prompted several target design studies to determine the optimum parameters for a demonstration of scientific breakeven using electron beam driven pellet fusion. However, little work has been reported on target designs that match present accelerator parameters. If targets could be designed for existing machines, then a greater understanding of the beam target interactions and implosion physics could be gained, allowing refinement of designs for future machines and targets. One of the major difficulties in designing this type of pellet is the long pulse width characteristic of existing machines, typically greater than 50 ns. Published fusion breakeven designs require pulse lengths of the order of 5 ns to efficiently compress and heat the DT fuel; longer implosion times allow the gas to cool through thermal conduction to the walls, degrading the maximum values of density and temperature in the fuel.

*Research performed under the auspices of the U. S. Energy, Research and Development Administration, Contract No. W-7405-ENG-48.

It is the purpose of this paper to present a design that would produce burn conditions in a pellet imploded by present-day long pulse accelerators.

II. Target Description

The range of parameters considered for this design were restricted to beam voltages of 1 MeV and pulse widths of 50 ns, with zero rise and fall time. Total beam energy was varied from 10 KJ to 100 KJ.

Figure 1 shows the target geometry and the configuration of the incoming beam. The target is characterized by a relatively large diameter, i.e., 1 cm, and a shell thickness equal to one-third the classical range of 1 MeV electrons. The interior of the shell is filled with low density DT gas and the shell itself is composed of either gold, copper, or lithium. The electron beam is also 1 cm in diameter and is restricted to flow in the axial direction, with a uniform current density in the radial dimension. The advantages of using a larger beam include: 1) relaxation of the superpinch requirement and 2) a larger energy content of the incoming beam compared to a superpinched beam.

The thin shell of the target allows one to use a different mechanism for imploding the capsule than suggested for breakeven targets. The shell itself acts as an isothermally-heated pusher causing faster implosion velocities than would be attainable from a shell with a thickness equal to a classical range. The

shell allows the 1 MeV electrons to penetrate to the fuel; and, in fact, a large portion of the incident beam passes right through the target. The result is an axially flowing current through the pellet which both heats the plasma and forms a B_θ field inside the shell. This concept was first suggested by Physics International[1] and separately reported by Rudakov of the Kurchatov Institute.[2]

The existence of the magnetic field depends strongly on the location and magnitude of the return current. If the return current flows through the fuel region, the magnetic field inside the shell is greatly reduced. However, if the return current flows outside the gas, several effects become important. Normally, a long input pulse would allow the gas to cool by thermal conduction to the shell wall as the pellet is imploding. The net magnetic field coupled to the beam-heated plasma reduces the thermal conduction to the wall, which for this design, is the maximum loss term. The self-field of the beam can also increase the alpha deposition at burn time if the Larmour radius of the alpha particles is less than the radius of the sphere of fuel. Thus, the incident beam explodes the shell, preheats the gas and, depending on the return current path, can reduce thermal conduction to the walls, and increase alpha deposition.

III. Electron Deposition

To ensure the implosion of the target occurs with good symmetry, one must determine the proper shell thickness and material that allows the beam to uniformly heat the shell and

still deposit a significant fraction of the input energy. Figure 2 shows the three materials studied as a function of shell thickness. The electron deposition was investigated with SANDYL, an electron-photon Monte-Carlo transport code. The sphere was divided into eight sections and the electron source was represented as a disc with axially-directed uniform emission. As noted in Figure 2, the gold shell did not provide sufficient uniformity of beam deposition unless thicknesses of the order of 10 μm were used. However, a 10 μm shell allows deposition fractions less than 1%, far too inefficient for the low energy beam being considered. The best material appears to be Lithium, as it has a very low scattering angle for 1 MeV electrons, allowing the beam to pass through the shell essentially unchanged in direction, but the shell still absorbs a large fraction of the beam energy. The deposition profiles for a Lithium shell 1.0 mm thick are shown in Figure 3. Each line represents a segment of the sphere and the profiles are normalized to the mass of the segment. The abscissa is incremented in tenths of a millimeter, representing steps in shell thickness.

IV. Electron Beam Heating of the Fuel

To determine the heating effects of the incoming electron beam, LASNEX, a laser-fusion implosion code, was run with the hydrodynamic motion turned off. The resulting fuel temperatures represent beam heating only, as there was no compression by the shell. These temperatures are tabulated in Figure 4 as a function of beam input energy for the Lithium shell. Although only a few eV of preheat exists, adiabatic compression of the gas would cause significant ion temperatures in the fuel.

V. Effect of Magnetic Field

Although true adiabatic compression cannot be achieved at these beam energies and implosion times, the thermal losses can be greatly reduced by the magnetic field induced by the penetrating beam. The equations shown in Figure 5 relate the effect of plasma parameters and applied magnetic field to the thermal conduction losses. Equation 1 describes the component of heat flow due to electron conduction with the second term on the right-hand side representing transport perpendicular to the magnetic field. The coefficient, $K_\perp$, is defined in terms of $\omega_e\tau_e$ in Equation 2 and after inserting the definitions of ω_e and τ_e a form of $K_\perp$ is obtained, showing the dependence on magnetic field, temperature and density. Heat flow due to ion conduction has a similar form and the perpendicular component for the ion term is given in the last equation.

A plot of K_e and $K_\perp$ is shown in Figure 6 as a function of $B\Theta^{3/2}/\rho$ and one notes a hundred-fold decrease in K_e for $B\Theta^{3/2}/\rho = 40$, denoted by point A. For an assumed density of 10^{-7} g/cc and a plasma temperature of 3 eV, this corresponds to a magnetic field of 27 KG or a beam current of 68 KA. This is well within present machine capabilities and therefore an axial beam should reduce the thermal losses. Larger values of magnetic field cause a reduction in the ion conduction term as well, and the highest beam current assumed reduces the conduction loss to values shown at point B.

One question that must be addressed is the diffusion time of the magnetic field through the shell. Using the conductivity of Lithium at room temperature yields a diffusion time of the

order of 1 s, long compared to typical implosion times of 150 to 350 ns. Thus the field remains trapped in the plasma long enough to prevent thermal losses during implosion.

If the magnetic field is sufficiently strong, deposition of the 3.5 MeV alpha particles produced by the DT burn will be affected. Since the Larmour radius of the alpha particle is inversely proportional to the magnetic field, the deposition will depend strongly on the current of the incoming beam. For an initial shell radius of .5 cm, current values above 2.5 MA are required to reduce the loss of alphas from the fuel region. Thus this term will be important for only the very highest energy levels considered.

VI. LASNEX Runs

Implosion calculations using LASNEX were done as shown in Figure 7. Total beam energy was assumed for an incoming flux of 1 MeV electrons with a 50 ns pulse width. The current intercepted by the gas was then calculated geometrically and checked with SANDYL predictions. This current value was used to obtain the magnetic field and K_e and K_i were then determined using $\rho = 10^{-7}$ g/cc and the temperature from the LASNEX runs with the hydro turned off. LASNEX was rerun with the new K_e and K_i to determine the new temperature and the process was repeated until a self-consistent temperature and thermal conduction multiplier was found. One dimensional LASNEX runs were then made with these parameters to determine the thermonuclear yield. Figure 8 shows the expected output from a 0.1 cm thick

Lithium shell as a function of input beam energy. The family of curves represent different gas densities and corresponding values of K_e and K_i. One notes that an observable flux of neutrons can be obtained from a beam input energy as low as 20 KJ. The range of data shown in Figure 8 extends from 10^2 neutrons at 10 KJ to 7×10^{10} neutrons at 100 KJ. The values of density shown in Figure 8 indicate peak yield occurs at $\rho = 10^{-7}$ g/cc; however, this density requires a large compression ratio and thus a more stringent beam uniformity than the target with $\rho = 2 \times 10^{-5}$ g/cc. Therefore, if beam irregularities cannot be removed, the higher density pellet is suggested even though lower outputs are predicted.

Figure 9 shows the output as a function of shell thickness with the optimum occurring with 0.09 cm of Lithium. Again, the abscissa represents input beam energy. Although the implosion velocity should increase as the shell thickness is reduced, the thinner shells absorb much less of the incoming beam and therefore do not provide as much output.

Output characteristics for the optimum Lithium shell design are shown in Figure 10. The highest values of ion temperature noted are 2 keV with implosion velocities of 4 cm/us. The densities obtained at maximum compression are .2 g/cc, yielding a ρr of .001 g/cm^2. The time to maximum compression is typically several hundred nanoseconds due to the large shell diameter and low implosion velocity; but this is desirable as it removes the

uncertainty of the neutron flux being caused by beam target interactions.

VII. Comparison with Two-Beam Irradiation

The approach just described was developed for use with single beam accelerators as this configuration is characteristic of most existing machines. For comparison, a high Z pellet irradiated on both sides as is possible on a HYDRA-type machine was also investigated. The target consisted of a 60 μm gold shell with an inner radius of 0.5 cm and a DT gas fill with $\rho = 10^{-7}$ g/cc. Conduction terms were left unchanged as there is no net beam current through the gas in this geometry. Results are plotted in Figure 11, again as a function of total beam energy. At very low beam energies, the two-sided irradiation provides a larger thermonuclear yield, but this drops off above 20 KJ as the thermal conduction terms become important. The third curve is a plot of a 3 mm diameter pellet which yields the highest output at low energies but also requires that the same beam energy be made available in an area approximately 10 times smaller than the 1.0 cm diameter beam.

VIII. Conclusions

In conclusion, by using a thin shell of low Z material, the electron beam can be used to both preheat a DT gas and reduce thermal conduction. This allows implosion dynamics to be studied on present electron beam accelerators without a strong superpinch condition and using only one beam. Caution is suggested

however, as uniformity of the incoming beam must be within a few percent to obtain yields as predicted by our calculations.

Further, this approach is predicated on reduced thermal conduction to the walls, a condition that will not occur if the return current path is through the center of the pellet.

REFERENCES

1. Physics International, Inc., private communication.

2. Babykin, M. V., Ye. K. Zavoisky, A. A. Ivanov, I. I. Rudakov, Nuclear Fusion, Supplement 1972, pp. 75.

FIGURE CAPTIONS

Fig. 1: Target description and configuration of incoming electron beam.

Fig. 2: Uniformity and deposition data for axial electron beam passing through lithium, copper, and gold shells of varying thickness.

Fig. 3: Deposition profile as a function of radius for a 1 mm thick lithium shell. The sphere is divided into eight sections with each curve representing the deposition in one section.

Fig. 4: Predicted temperatures of D-T gas heated by electron beams of varying energy.

Fig. 5: Equations describing heat conduction in plasma. The pertinent terms are $K_{e_\perp}$ and $K_{i_\perp}$ expressed as functions of $BT^{3/2}/\rho$. The results are from Braginskii, Reviews of Plasma Physics, Vol. 1.

Fig 6: Perpendicular thermal conduction terms vs. $BT^{3/2}/\rho$. Point A represents $BT^{3/2}/\rho$ = [illegible] where $K_{e_\perp} = K_{i_\perp}$; point B represents $BT^{3/2}/\rho$ = [illegible], the largest value considered.

Fig. 7: Input values for LASNEX. The beam energy is selected first, yielding the total beam current. The magnetic field is derived from the portion of the current in the gas and then $BT^{3/2}/\rho$ is calculated from the temperatures listed in Fig. 4. Finally, K_e and K_i are determined from $BT^{3/2}/\rho$, and these values are used to find the new temperature.

Fig. 8: Neutron output vs. electron beam energy for various gas densities. The target is a 1 mm thick lithium shell.

Fig. 9: Neutron output vs. electron beam energy for various shell thicknesses. The D-T density is fixed at 10^{-7} g/cc.

Fig. 10: Parameters for 1 mm thick lithium shell at 100 kJ and 20 kJ input energies. The neutron flux is chosen at the time of minimum fuel volume. Temperature, velocity, and density are maximum values.

Fig. 11: Neutron output vs. electron beam energy for various target designs. The lithium shell assumes a one-sided axial electron beam. The gold shells have uniform beam irradiation and differ only in shell diameter.

TARGET GEOMETRY

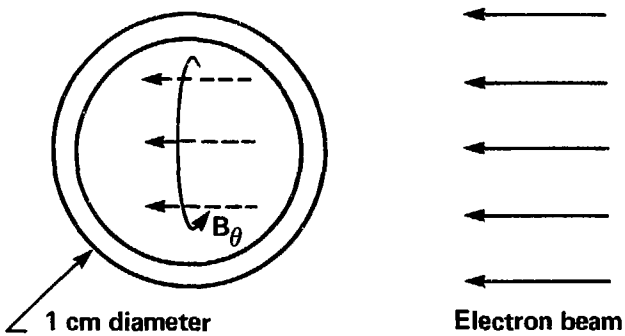

Target

- Low density D-T fill
- shell thickness $\leqslant$ 1/3 classical range for 1 MeV

Electron beam

- Axially directed, uniform current density
- Explodes shell
- Heats gas
- Creates B_θ in gas if $I_{return} < I_{beam}$
- Aids alpha deposition

Figure 1

BEAM DEPOSITION AND UNIFORMITY

Material	Shell thickness	Uniformity	% deposited
Lithium	0.5 mm	10%	25%
	1.0	15%	48%
	2.0	35%	80%
Copper	0.05mm	330%	24%
	0.10	580%	50%
Gold	0.01 mm	280%	8%
	0.02	400%	17%
	0.06	800%	25%

Figure 2

ENERGY DEPOSITION/UNIT MASS FOR 1 mm THICK LITHIUM SHELL

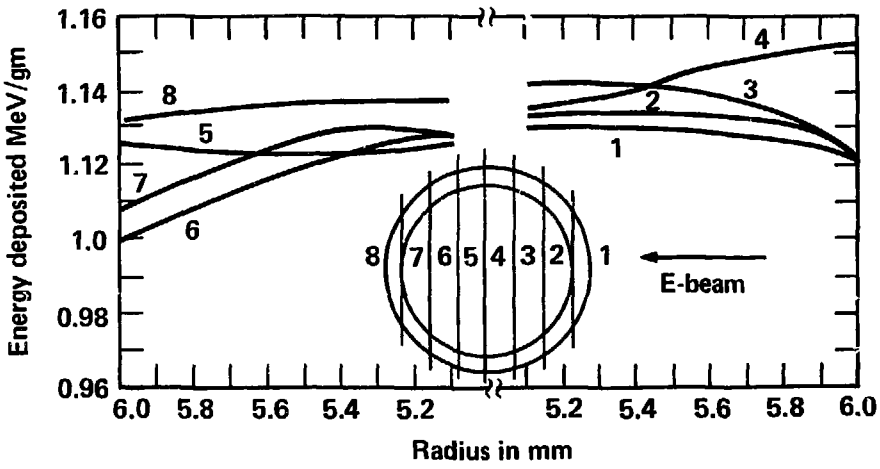

Figure 3

ELECTRON BEAM HEATING OF DT GAS

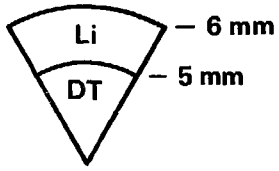

$\rho_{DT} = 10^{-7}$ g/cc

Electron beam energy (kJ)	Thermal conduction ON (eV)	Thermal conduction OFF (eV)
10	0.217	0.5
20	0.436	1.07
50	1.09	2.7
100	2.17	5.4

Figure 4

THERMAL CONDUCTION (BRAGINSKII)

$$Q_T^e = -K_{\parallel}^e \nabla_{\parallel} T_e - K_{\perp}^e \nabla_{\perp} T_e - K_{\Lambda}^e [h \nabla T_e]$$

$$K_{e_\perp} = \frac{n_e T_e \tau_e}{m_e} \left[\frac{4.7\, \omega_e^2 \tau_e^2 + 11.9}{\omega_e^4 \tau_e^4 + 14.8 \omega_e^2 \tau_e^2 + 3.77} \right]$$

$$= 4.66 \frac{n_e T_e}{m_e \omega_e^2 \tau_e} \quad \omega_e \tau_e >> 1$$

$$K_{e_\perp} T_e^{-5/2} = \frac{1.07 \times 10^{20}}{B T_e^{3/2} / \rho}$$

B in MG
T_e in keV
ρ in g/cc

$$Q_T^i = -K_{\parallel}^i \nabla_{\parallel} T_i - K_{\perp}^i \nabla_{\perp} T_i + K_{\Lambda} [h \nabla T_i]$$

$$K_{i_\perp} = \frac{n_i T_i \tau_i}{m_i} \left[\frac{2\omega_i^2 \tau_i^2 + 2.65}{\omega_i^4 \tau_i^4 + 2.7\, \omega_i^2 \tau_i^2 + .68} \right]$$

$$= \frac{2 n_i T_i}{m_i \omega_i^2 \tau_i} \quad \omega_i \tau_i >> 1$$

$$K_{i_\perp} T_i^{-5/2} = \frac{1.17 \times 10^{18}}{B T_i^{3/2} / \rho}$$

Figure 5

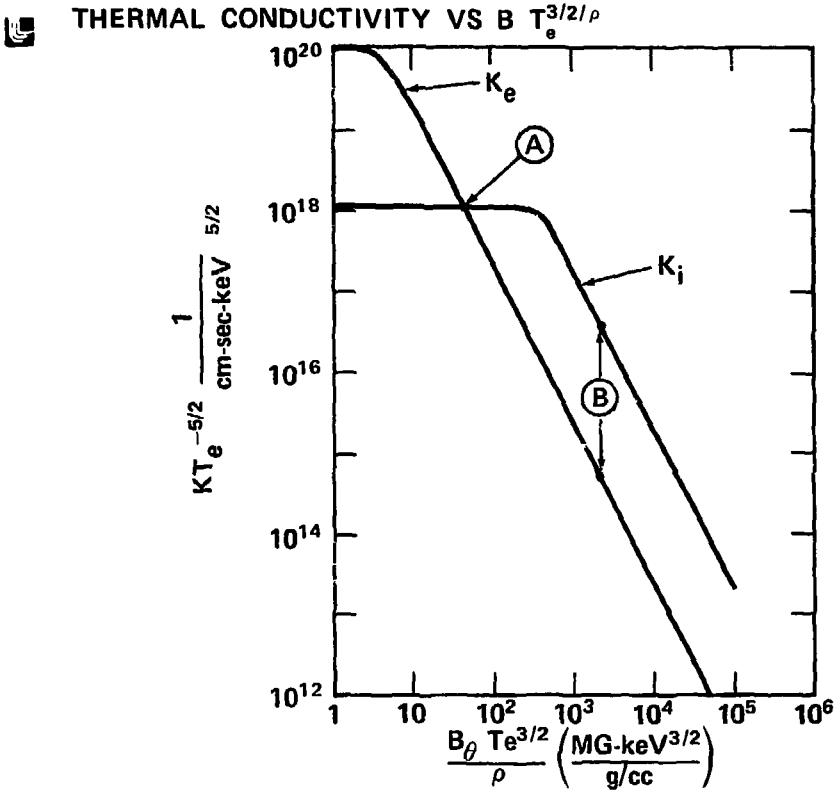
THERMAL CONDUCTIVITY VS B $T_e^{3/2}/\rho$
10^{20}
10^{18}
10^{16}
10^{14}
10^{12}
K_e
K_i
A
B
$KT_e^{-5/2}$ $\frac{1}{\text{cm-sec-keV}^{5/2}}$
1
10
10^2
10^3
10^4
10^5
10^6
$\frac{B_\theta\ Te^{3/2}}{\rho}$ $\left(\frac{\text{MG-keV}^{3/2}}{\text{g/cc}}\right)$

Figure 6

LASNEX INPUT

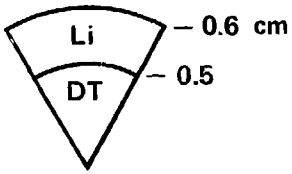

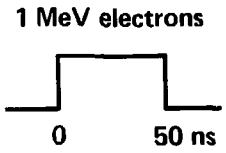

Beam energy	Total current	Current in D-T	B_θ	$\frac{B_\theta T_e^{3/2}}{\rho}$	k_e	k_i
10 kJ	0.2 MA	0.14 MA	0.06 MG	6.7	0.3	1.0
20	0.4	0.28	0.11	35	1.5×10^{-2}	1.0
50	1.0	0.70	0.28	400	1.4×10^{-4}	0.69
100	2.0	1.4	0.56	2200	4.8×10^{-6}	2.9×10^{-2}

Figure 7

NEUTRON OUTPUT VS ENERGY OF ELECTRON BEAM

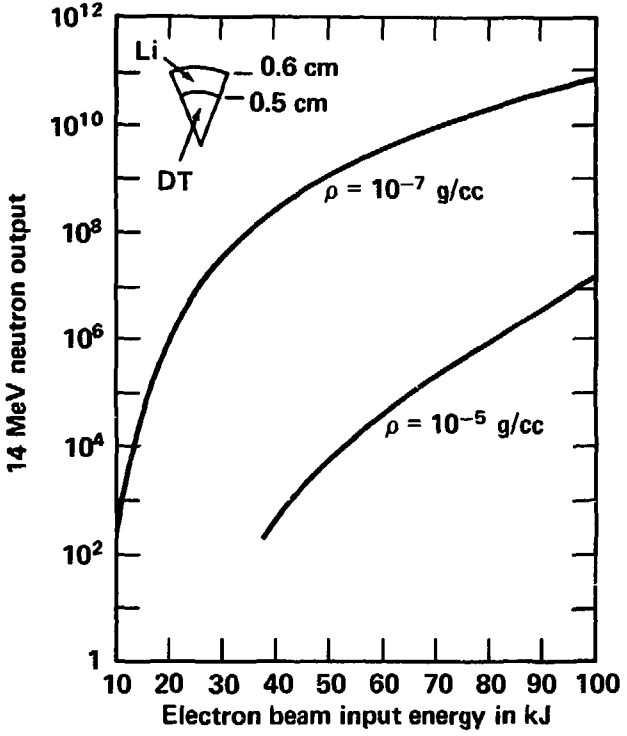

Figure 8

NEUTRON OUTPUT VS ENERGY OF ELECTRON BEAM

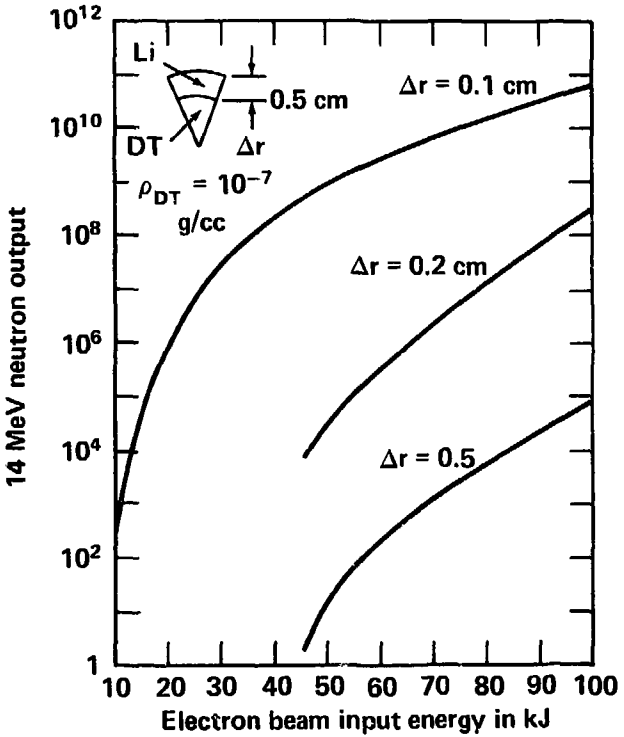

Figure 9

LITHIUM PELLET IMPLOSION CHARACTERISTICS

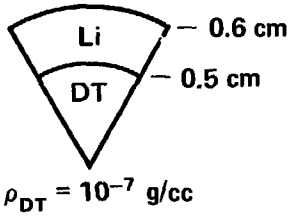

Beam energy	100 kJ	20 kJ
Energy absorbed	48 kJ	9.6 kJ
Yield	343 mj	3.77 μj
14 MeV neutrons	7×10^{10}	8.5×10^{5}
Ion temperature	2.4 keV	0.23 keV
Shell velocity	4.3×10^{6} cm/s	1.94×10^{6} cm/s
DT density	0.21 g/cc	2.1 g/cc

Figure 10

NEUTRON OUTPUT VS ENERGY OF ELECTRON BEAM

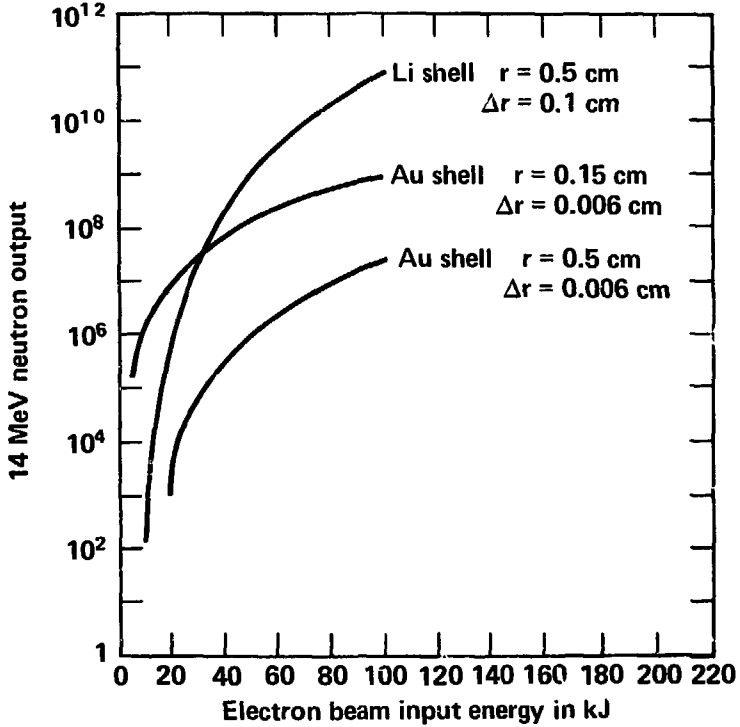

Figure 11